

Characterization of Barrett esophagus and esophageal adenocarcinoma by Fourier-transform infrared microscopy

Luca Quaroni^{*abc} and Alan G. Casson^c

Received 7th January 2009, Accepted 21st January 2009

First published as an Advance Article on the web 11th February 2009

DOI: 10.1039/b823071d

The objective of this exploratory study was to evaluate the feasibility of using Fourier-Transform Infrared (FTIR) spectromicroscopy to characterize formalin-fixed, paraffin-embedded human esophageal tissues. Matched histologically normal esophageal squamous epithelium (NS), premalignant Barrett esophagus (BE), and primary esophageal adenocarcinoma (EADC) tissues, each defined according to strict clinicopathologic criteria, were obtained from patients who underwent esophageal resection. Using confocal IR microscopy, measurements in the mid-IR spectral region were carried out in transfection configuration, scanning regions of interest in 15 µm steps. A multidimensional dataset reporting the spectroscopic properties at each sampled point were analyzed by performing a hierarchical cluster analysis on the second derivative of spectral traces. Normal esophageal epithelia were characterized by a few well defined regions, mostly of large size (tens of contiguous pixels), which correlated with tissue histology, specifically the basal cell layer. BE tissues had characteristic regions localized to gland crypts, ranging in size from one pixel to a few tens of pixels, which displayed IR spectra with defined absorption features characteristic of glycoproteins. The incorporation of synchrotron light to improve the resolution of individual cells in BE tissues has demonstrated that these glycoproteins are associated with goblet cells, the characteristic cell type defining BE. Whereas the highly fragmented regions identified in EADC likely reflect tumor heterogeneity, FTIR mapping would appear to be a potentially useful technique to identify premalignant BE tissues. The technical feasibility of using FTIR to characterize formalin-fixed, paraffin-embedded human esophageal tissues demonstrates the potential of this technique to study archival human BE tissue specimens via automated screening techniques.

Introduction

Over the past three decades, a marked change in the epidemiology of esophageal malignancy has been reported in many Western populations, with an increasing incidence of esophageal adenocarcinoma (EADC).¹ While the reasons for this trend are unknown, chronic gastroesophageal reflux disease (GERD) and several lifestyle risk factors, including obesity and diet, tobacco and alcohol consumption, have been implicated.^{2–6} Primary EADC generally arises from Barrett esophagus (BE), an acquired condition predisposed by GERD, in which the normal esophageal squamous epithelium is replaced by a specialized metaplastic columnar cell-lined epithelium.^{7,8} Progression of BE to invasive EADC is reflected histologically by the Barrett metaplasia-dysplasia-adenocarcinoma sequence, and several critical molecular genetic alterations have now been identified at various stages of progression.^{9–11}

Despite recent advances in multimodality therapy, the prognosis for invasive EADC remains generally poor. It therefore seems likely that significant progress with this malignancy will only

be made with a clearer understanding of its tumor biology, and early diagnosis through endoscopic screening and surveillance programs.⁷ The histopathologic finding of dysplasia (particularly high-grade dysplasia, HGD) in esophageal biopsies obtained at endoscopy is still considered the most reliable predictor of malignant progression, but accurate grading of dysplasia is somewhat subjective; as a consequence, inter- and intra-observer variation remains high.^{7,12–14} Recent studies have therefore explored the role of molecular biomarkers to improve the diagnostic accuracy of dysplasia and to predict individuals at increased risk for esophageal malignancy.^{15–17} However, none, to date, have routinely been incorporated into current clinical practice.

The potential of Fourier-Transform Infrared (FTIR) spectroscopy as a diagnostic technique has been recognized for decades.^{18,19} Absorption of radiation in the mid-infrared spectral region provides rich information on the molecular properties of the sample, in particular regarding composition. Most molecular species absorb infrared light, giving rise to characteristic spectral patterns in transmitted light.²⁰ Many pathological conditions are associated to perturbations of metabolism that are reflected in homeostatic changes of molecular components in cells and tissues. The clinical potential of FTIR spectroscopy to detect such changes and its use as a diagnostic tool has therefore recently received increasing attention.^{21–29}

Recent work by Wang *et al.*³⁰ has shown that FTIR spectroscopy in the Attenuated Total Reflection (ATR) configuration

^aCanadian Light Source Inc., 101 Perimeter Road, Saskatoon, SK, Canada S7N 0X4

^bDepartment of Chemistry, University of Manitoba, Parker Building, Winnipeg, MB, Canada R3T 2N2

^cDepartment of Surgery, Royal University Hospital, 103 Hospital Drive, Saskatoon, SK, Canada S7N 0W8

Published on 11 February 2009. Downloaded by Michigan State University on 24/01/2016 23:45:44.

can be used to identify dysplastic and non-dysplastic (metaplastic) change in BE, resulting in reduced inter-observer variation between two gastrointestinal histopathologists, and therefore improved diagnostic accuracy for dysplasia. In addition, this technique was used to quantify infrared spectral components of histologically normal esophageal squamous epithelia and gastric mucosa. However, these measurements provided limited spatial resolution in the horizontal plane, preventing the assignment of spectral properties to sample regions smaller than a few hundred microns. As a consequence, past attempts to perform FTIR on even small biopsy samples for diagnosis have provided contentious results, arising from the fact that macroscopic FTIR measurements average out the response of several hundred cells.^{25,31–35} This allows the possibility that observed spectral properties may be dominated by the response of various cellular and tissue types that typically exist within human premalignant and malignant tissues. Under such conditions the response from minority components which display distinct histopathologic characteristics may go undetected.

In this exploratory study, we utilized FTIR spectroscopy in the microscopy optical configuration to evaluate and compare samples of histologically normal esophageal squamous epithelium (NS), BE, and primary EADC tissues, with high spatial resolution, and to match these features to specific cellular areas in corresponding histologic tissue sections. We initially used FTIR mapping with a globar light source followed by hierarchical clustering analysis to identify regions of the sample with spectral features characteristic of the histopathology. We then used a synchrotron light source to perform diffraction-limited FTIR mapping of single goblet cells, the characteristic histologic feature of intestinal metaplasia, the hallmark of BE.

Experimental

Esophageal tissues

Esophageal tissues were obtained with informed, written consent from a well characterized series of patients enrolled in a study of the molecular pathogenesis of EADC.^{36–38} Approval for this study was granted by the Capital Health Research Ethics Board (QE-2000-277), and tissue samples were collected in accordance with the 1998 Canadian Tri-Council Policy ‘Statement on Ethical Conduct for Research Involving Humans’. No patient received induction (preoperative) chemotherapy or radiation therapy, and immediately following surgical resection (esophagogastrectomy), esophageal tissues were formalin-fixed and paraffin-embedded according to standard protocol in the Department of Pathology, QEII Health Sciences Centre, Halifax, Nova Scotia, Canada. Haematoxylin and eosin (H&E) stained tissue sections (4 µm in thickness) were examined in collaboration with two consultant gastrointestinal histopathologists, to define representative sections of the primary tumor, adjacent BE (characterized by intestinal metaplasia), and histologically normal esophageal squamous epithelium at the site most distant to the primary tumor. Strict clinicopathologic criteria were used to define adenocarcinomas of primary esophageal origin (EADC), thereby avoiding misclassification with adenocarcinomas arising at the esophagogastric junction or from the gastric cardia, as follows: (1) the presence of an associated BE, (2) more than 75% of the

tumor mass involving the tubular esophagus, (3) direct invasion of periesophageal tissues, (4) minimal gastric involvement, and (5) clinical symptoms of esophageal obstruction (dysphagia).

Unstained esophageal tissue sections, immediately adjacent to H&E stained sections, 7 µm in thickness, were deposited on low-emittance slides (Kevley Technologies, Chesterland, OH) and used for IR mapping experiments.

FTIR spectromicroscopy and mapping

FTIR mapping experiments were carried out using the endstation of beamline 01B1-01 at the Canadian Light Source. The endstation comprises a Bruker (Bruker Optics, Billerica, MA) IFS66v/s interferometer coupled to a Hyperion 2000 IR microscope. Low resolution IR maps were measured using the internal globar source of the interferometer. Maps with diffraction-limited resolution were recorded using synchrotron light.

All FTIR mapping experiments were carried out in transfection. A 36× magnification Schwarzschild objective was used to focus IR light on the sample and collect the reflected beam. A KBr-supported Ge multilayer beamsplitter and an MCT detector were used to measure spectra in the mid-infrared spectral region. Interferograms were recorded by scanning the moving mirror at 40 kHz, to an upper frequency limit of 7900 cm⁻¹, and with a spectral resolution of 4 cm⁻¹. Single channel traces were obtained using the fast Fourier-transform algorithm, without any zero-filling, after applying a Blackman-Harris 3-Term apodization function.

Maps were recorded by raster scanning the sample using a mechanized stage. Spatial resolution was defined by closing a confocal aperture positioned after the sample plane. For low resolution maps the confocal aperture was set at 15 µm × 15 µm and the stage stepped by 15 µm in both X and Y directions; 32 scans per point were collected at a 40 kHz data acquisition frequency. For diffraction-limited maps, the confocal aperture was set at 4 µm × 4 µm and the stage stepped by 2 µm; 128 scans per point were collected at a 40 kHz scan rate.

For single point spectra, the confocal aperture was set at 4 µm × 4 µm; 512 scans per point were collected at a 40 kHz scan rate.

Infrared maps were constructed by calculating the second derivative of the spectral traces with 13-point Savitzky-Golay smoothing. The amplitude of the negative peak of the second derivative was mapped over the surface of the sample without any additional baseline correction. The program OPUS, version 6.5 (Bruker Optics, Billerica, MA), was used for data processing and analysis, except for what concerns clustering analysis (see below).

Hierarchical clustering analysis was carried out using the program Cytospec (CytoSpec Inc., Boston, MA) on the second derivative of spectral traces in the 930–1300 cm⁻¹ region. Spectra were compared using Pearson’s function and classified in clusters using Ward’s algorithm. The number of clusters was varied from 3 to 12.

Results and discussion

For each patient, we evaluated histologically normal esophageal squamous epithelium, BE and EADC within the same tissue section, thereby avoiding potential differences in tissue

processing (source, preparation and storage). We first produced infrared maps of unstained esophageal tissue sections, and compared these with matched tissue sections stained with H&E. Infrared absorption maps were recorded by raster scanning the sample in the focal plane of an IR microscope, using $15\text{ }\mu\text{m} \times 15\text{ }\mu\text{m}$ apertures and $15\text{ }\mu\text{m}$ steps.

Specific features in cellular and tissue samples were mostly expressed by subtle changes in band intensity and structure, within a complex pattern of absorption bands and other spectral structures due to optical effects rather than absorption. Overall, nearly 600 infrared absorption spectra were recorded to

characterize one set of samples, preventing a detailed analysis of specific features on a spectrum by spectrum basis. To overcome this problem we resorted to the use of multivariate clustering analysis to reduce the dataset to clusters of spectra with related properties. As multivariate methods are generally very responsive to subtle variations in composition, we used unsupervised hierarchical clustering analysis as an image reconstruction method to identify regions with high similarity within each resulting FTIR map.

Fig. 1 shows the results of the analysis performed on the FTIR maps using the spectral interval from 930 to 1300 cm^{-1} . This

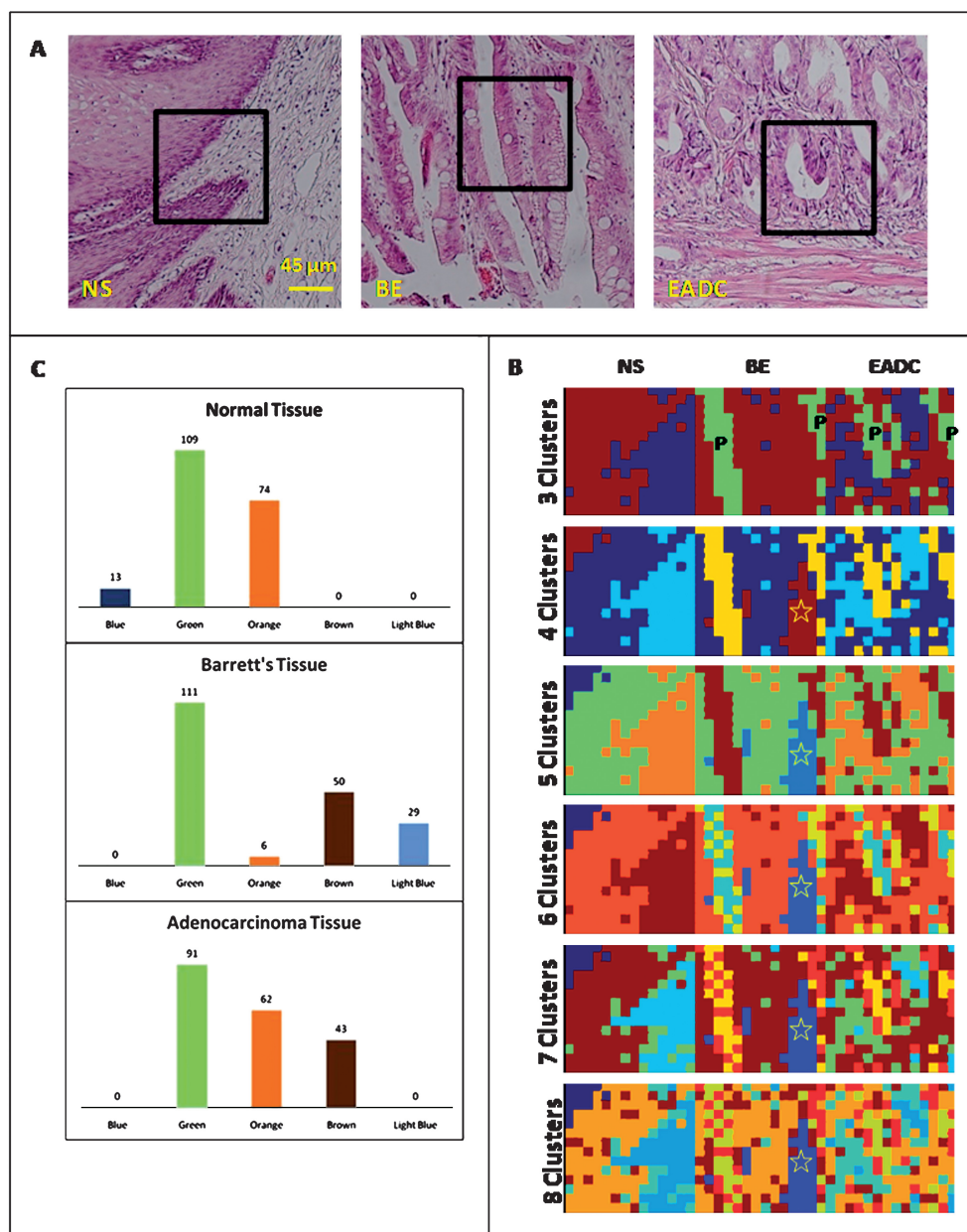


Fig. 1 (A) Visible light microscope image of the matched sections stained with haematoxylin and eosin. The frames indicate the portions of the matching section that were mapped with IR light. (B) Hierarchical clustering analysis of IR maps, calculated using an increasing number of clusters. The letter P indicates clusters representing paraffin only. The star indicates the largest cluster characteristic of BE tissue. 1 pixel = $15\text{ }\mu\text{m}$. (C) Number of pixels per region obtained from a 5-region clustering analysis. The color scheme of the columns matches the color scheme of the clusters in the 5 Cluster map. The 'Blue' cluster is observed only in NS tissue, while the 'Light Blue' cluster is observed only in BE tissue. The 'Brown' cluster corresponds to paraffin.

interval was selected to exclude the strong peaks resulting from paraffin at 1380 and 1470 cm⁻¹, thereby avoiding differentiating sample regions on the basis of variations in the local concentration of paraffin. This decision also excluded Amide I and Amide II bands from the clustering analysis. This was justified on the basis of two considerations. First, according to the study by Wang *et al.*³⁰ the absorption features associated with BE are all located in the spectral region between 800 and 1300 cm⁻¹, suggesting that Amide I and Amide II absorptions are not critical for the identification of BE tissue. Second, the absorption due to the Amide III vibration, at 1240 cm⁻¹, was still retained within the spectral region used for the analysis, thereby ensuring that local variations in protein concentration were still accounted for. To reduce the contribution of baseline variations, second derivative spectra were used for the clustering analysis.

Pixels were classified using an increasing number of clusters, from a minimum of 3 to a maximum of 12 (shown only up to 8 clusters in Fig. 1). The maps from each of the three different tissue sections were integrated into a single file, to allow the identification of similarities between regions in different tissues.

As expected, using three clusters for classification immediately identified portions of the sample that contained only paraffin, whereas portions corresponding to tissue were clustered into the two other classes (Fig. 1B). No regions containing pure paraffin are located in the healthy tissue portion. In BE and EADC sections, accumulations of paraffin are observed as very clear topographical features defining the lumen of crypts, where no tissue is present (the green color in the 3 Cluster maps of Fig. 1B).

Increasing the number of clusters allowed further differentiation of various other areas within each section. Areas of pure paraffin fragment into several different clusters, probably because of irregularities in the thickness of the paraffin layer. In contrast, few well defined regions characterize the tissue portion of the samples and are already well defined when using a total number of five clusters. Increasing the total number of clusters above five does not identify any new extended regions within the tissue sections. Using seven clusters allows differentiating pixels at the rim between previously defined regions, while increasing the number of clusters above seven fragments most of the regions into individual pixels corresponding roughly to individual cells. With such a high number of clusters, with pixels corresponding roughly to the size of a single cell, topographical issues and the positioning of each pixel relative to individual cells become all differentiating factors in the clustering analysis. Little additional information can be extracted on differences in chemical composition. For this reason we focused our analysis on maps analyzed with five clusters.

In 5 Cluster maps, normal esophageal squamous epithelium was described by only three of the clusters. Their second derivative spectra are shown in Fig. 2A (orange, green and blue clusters). These appeared overall compact and well layered, in agreement with the known structure of healthy esophageal epithelium. Two of these clusters were also observed in BE and EADC tissues, although they appeared fragmented and irregular, with pixels of the same cluster being distributed throughout the tissue. This was particularly marked in EADC tissues. One of these clusters was only observed in healthy tissue, as a compact layer of cells (blue in the five cluster map). The main differences between the spectra of orange and green clusters in Fig. 2A is the

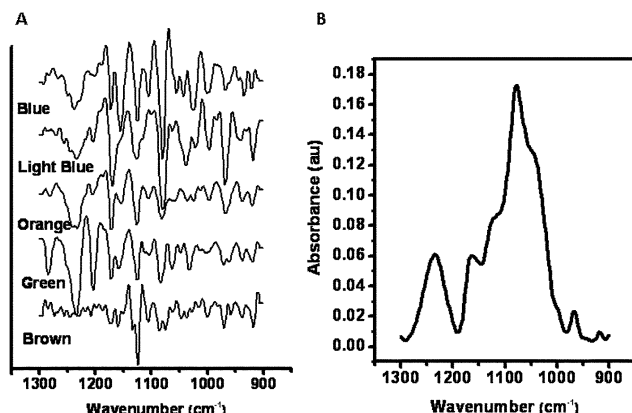


Fig. 2 Average spectra of the regions detected by hierarchical analysis with five clusters and their second derivatives. (A) Color entries beside the spectra indicate the color coding of the corresponding cluster. The brown cluster corresponds to paraffin; the light blue cluster is the Barrett cluster. (B) Detail of average spectrum of the Barrett cluster.

contribution of the absorption at 1240 cm⁻¹. This band is generally assigned to the Amide III vibration from peptide groups in proteins and the overlapping antisymmetric stretching vibration of phosphodiesters.³¹ The second derivative spectrum of the blue cluster displays strong bands at 1029 cm⁻¹, 1079 cm⁻¹, and 1150 cm⁻¹. Glycogen, one of the most abundant cellular components that can contribute strong absorption bands in this spectral region, has characteristic peaks at 1028, 1078, and 1151 cm⁻¹, suggesting that its accumulation is responsible for the distinguishing spectral features of this cluster. The presence of large concentrations of glycogen is a feature of mature cells in epithelial tissue, with a decreased concentration being often associated to dysplastic processes.³⁹ Indeed, the detection of varying spectral contributions from glycogen has been proposed as one of the parameters that allow discriminating healthy from BE tissue using FTIR spectroscopy.³⁰ Overall, the pattern of spectroscopic changes observed in healthy tissue can be described by a variation in the contribution from glycogen and phosphodiesters (presumably from nucleic acids). This pattern of spectroscopic changes has already been reported in the study of cervical epithelium, and has been attributed to the different stages of cell maturation going from the stroma, through the basal and pre-basal layers, up to the superficial layer.^{39,40}

One well defined cluster differentiated BE from each of the other tissues studied. The pixels of this cluster were always located on the gland rims and appeared as compact and continuous threads or as scattered pixels on the edge of the gland lumen. This cluster retained its identity when the number of regions was increased, and did not differentiate even when ten regions (not shown) were used for the classification, indicating that its spectral features were markedly distinguished from the ones of other clusters in the sample. The cluster was completely absent from portions of normal esophageal squamous epithelium. Comparison with the visible light image of the matched stained section shows that the cluster corresponded to gland rims where goblet cells were observed. This was designated the 'Barrett cluster'.

Fig. 2A shows the average second derivative spectra associated with the BE epithelium (light blue cluster). The principal spectral

feature unique to BE appeared to be the structure of the complex multiplet of absorption bands between 1000 and 1300 cm⁻¹. The multiplet was characterized by components peaking at 1080 cm⁻¹, 1124 cm⁻¹, and 1171 cm⁻¹. A separate strong and broad band was also observed around 1240 cm⁻¹, accompanied by a weaker but well resolved band around 970 cm⁻¹.

Absorption bands at 1080 cm⁻¹, 1124 cm⁻¹, and 1171 cm⁻¹ are characteristic of the C–O and PO₂ stretching vibrations of oligo- and poly-saccharide molecules. The band at 970 cm⁻¹ is also a characteristic vibration of phosphodiester groups.³¹ The same spectral pattern of Fig. 2B was also reported by Wang *et al.* in their work on ATR analysis of macroscopic tissue samples from patients with BE. It was concluded that these spectral features are characteristic of tissue histology, and matched the absorption of the glycoprotein mucin.³⁰

Glycogen in human tissue often contributes a strong multiplet to this spectral region. However, the difference in peak positions, and in particular the clear absence of the strongest of glycogen peaks, at 1028 cm⁻¹, rules out a substantial contribution from this biomolecule to the spectrum of the BE cluster, and supports the assignment of the multiplet to glycoprotein absorption.

The association between glycoprotein absorption bands and BE reported by Wang *et al.*³⁰ is therefore confirmed by our present study. In addition, by using IR microscopy, we also demonstrate that these absorption features are localized to the edge of crypts, in regions rich in goblet cells, suggesting a correlation between the presence of the latter and the accumulation of glycoproteins.

To explore the association between goblet cells and glycoprotein absorption bands we recorded IR maps of individual goblet cells. Goblet cells are about 10–30 μm in size and therefore appeared as a single pixel at the spatial resolution afforded by the experiments in Fig. 1. We therefore utilized mapping with high brightness synchrotron IR light to create an IR map of a single goblet cell with diffraction-limited spatial resolution. Representative maps are shown in Fig. 3. To reduce interference from baseline irregularities, maps were constructed by plotting the distribution of amplitude of the second derivative of the absorption spectra. The second derivative of an infrared absorption band, with a typical Gaussian/Lorentzian bandshape, is a sharp negative band with two weaker positive sidebands. FTIR maps were constructed by plotting the amplitude of the

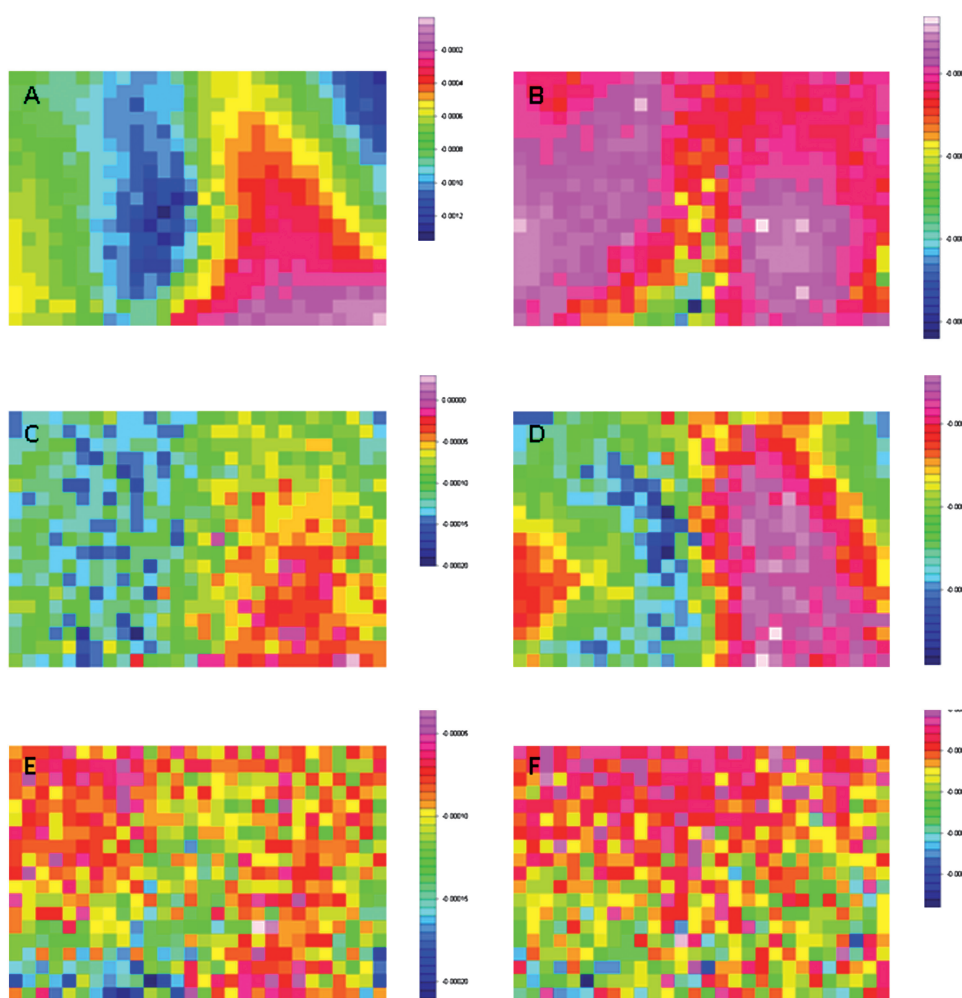


Fig. 3 Infrared maps of a single goblet cell. Images constructed by plotting the intensity at a given wavenumber in second derivative spectra. One pixel corresponds to 2 μm. (A) 1650 cm⁻¹; (B) 1688 cm⁻¹; (C) 1243 cm⁻¹; (D) 3290 cm⁻¹; (E) 1171 cm⁻¹; (F) 1080 cm⁻¹. The lower side of the maps is the crypt side.

central negative component of the second derivative. Therefore, in these plots larger negative values correspond to higher absorbance (darker shades of blue).

The goblet cell is characterized by a strong absorption at 1650 cm^{-1} , corresponding to the peak of the Amide I vibration, indicating a very high protein content within the goblet cell itself, higher than other portions of the cell. A shoulder was also observed on the high frequency side of the Amide I band in several spectra. With maximum intensity at 1688 cm^{-1} , this shoulder would correspond to a strong absorption from the carbonyl group of nucleic bases. This spectral feature appears to be localized to one region about $5\text{--}10\text{ }\mu\text{m}$ wide, on one side of the goblet cell, suggesting the potential location of the cell nucleus.

An absorption band at 1240 cm^{-1} was also distributed within the location of the goblet cell, as shown in Fig. 3C. This band was assigned to an overlapping contribution from the antisymmetric stretching absorption from phosphate and the Amide III vibration of polypeptides and co-localized with the Amide I band mapped in Fig. 3A, confirming the presence of a large concentration of proteins. The wider spread within the distribution of this band can be ascribed to the longer wavelength and corresponding decrease in spatial resolution.

Fig. 3D shows the distribution of absorption at 3290 cm^{-1} , a frequency corresponding to the peak absorption of the Amide A vibration from polypeptides overlapped with the absorption from the stretching vibration of hydroxyl groups around 3400 cm^{-1} .²⁰ As expected, the resulting distribution approximates the combination of maps in Fig. 3A and 3B.

The most remarkable observation was that the absorption bands assigned to the oligosaccharide component of glycoproteins at 1080 cm^{-1} , 1124 cm^{-1} and 1171 cm^{-1} , plotted in Fig. 3E and 3F, did not correlate with the distribution of Amide I absorption within the goblet. These bands, although present, appeared to be weak within the goblet cell itself. In contrast, their amplitude relative to the Amide I band increased when moving away from the goblet cell towards the edge of the crypt.

Fig. 4 shows individual spectra recorded with longer scans in specific positions of the sample, and their location relative to the mapped area. Spectrum 1 was recorded away from the goblet cell and the crypt, and showed only weak bands in the range $1000\text{--}1200\text{ cm}^{-1}$. Spectrum 2 was recorded inside the goblet cell and showed increasing absorption within this range. However, it was only in Spectrum 3 that the multiplet at 1080 cm^{-1} , 1124 cm^{-1} and 1171 cm^{-1} appears as strong as in the spectrum in Fig. 2 (Light Blue cluster). Comparison of the spectra in Fig. 4 and the maps in Fig. 3 indicates that glycoproteins, although present in the goblet cell, are mostly accumulated outside of the cell towards the crypt side.

The use of tissue sections that were formalin-fixed and paraffin-embedded raises a number of technical issues related to the spectroscopic analysis, as the presence of paraffin absorption bands may be a cause of potential interference. In this work we have shown that excluding the spectral regions with the strongest paraffin absorption bands does not significantly limit our capability to perform a hierarchical clustering analysis of BE tissue. Additional concerns relate to tissue fixation, embedding and storage, which may also potentially alter the complement of biomolecules and subsequently the results of FTIR-based analysis. However, we have demonstrated that BE is associated to gross changes in molecular composition, leading to an

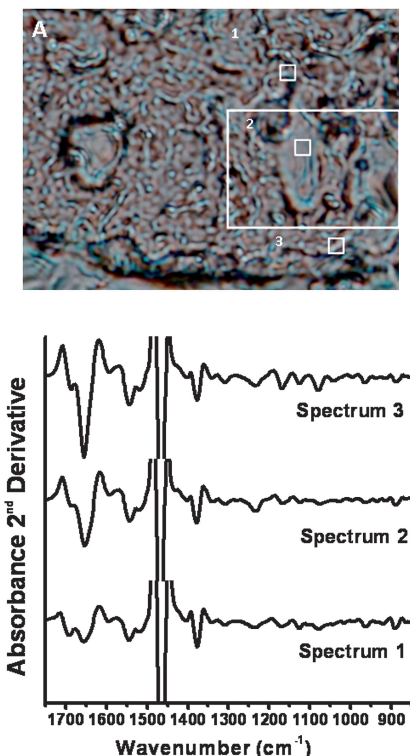


Fig. 4 (A) Visible light image of the sample region studied by FTIR mapping and spectromicroscopy with synchrotron radiation. The image was collected in reflection from a paraffin-embedded sample mounted on a MirrIR slide. The lower side of the maps is the crypt side. The white frame indicates the region of the sample which was mapped in Fig. 3. The square marks indicate the positions for single point measurements. (B) 2nd derivative of the spectra measured in points 1, 2 and 3. Bands due to paraffin have been allowed to go out of scale.

accumulation of glycoproteins and significant decrease in glycogen accumulation in the surface layer, and that these changes are easily detected by FTIR spectromicroscopy even after embedding. Our results using formalin-fixed, paraffin-embedded esophageal tissues are consistent with changes observed when fresh (unfixed) BE tissues were studied.⁴¹

An alternative strategy, using exfoliated cells from esophageal malignant and non-malignant tissues was reported by Maziak *et al.* who reported differences between esophageal carcinoma (tissue histology not stated) and normal epithelia.³² However, it is unclear whether such exfoliated cells are truly representative of the primary tissue type, considering the extent of cellular heterogeneity within tumor tissues, and the increasing role of the extracellular matrix in human carcinogenesis.^{42,43} This is particularly critical when using a technique such as FTIR spectroscopy, for which the capability to discriminate between various tissue types relies on its sensitivity to variations in molecular composition. Failure to provide a representative sample can involve altered relative abundance of some molecular components or their loss during the sampling procedure. These large changes in average molecular composition are easily greater than the subtle changes that accompany the onset of many pathological conditions, often localized to just a few cells. For these reasons, the reliability of FTIR diagnostics based on macroscopic samples of exfoliated epithelial cells has been questioned.^{39,40,44–46}

Using esophageal tissue sections in this study, no characteristic clusters specific to EADC were observed and we did not observe any specific spectroscopic changes associated with EADC. Within the limits set by spatial resolution, and the maximum number of clusters used, EADC tissue corresponded to a fragmented and irregular distribution of some of the clusters observed for normal esophageal and BE epithelia. This finding would be in keeping with the cellular heterogeneity frequently observed in many human solid tumors.

Conclusions

In conclusion, we have demonstrated the technical feasibility of using FTIR to characterize formalin-fixed, paraffin-embedded human esophageal tissues. Whereas the highly fragmented regions identified in EADC likely reflect tumor heterogeneity, FTIR mapping would appear to be a potentially useful technique to identify premalignant BE tissues, characterized by an accumulation of glycoproteins. The incorporation of synchrotron light to improve the resolution of individual cells in BE tissues has demonstrated that these glycoproteins are associated with goblet cells, the characteristic cell type defining BE.

Acknowledgements

Funded in part by the National Cancer Institute of Canada with funds from the Canadian Cancer Society. We wish to thank Dickran Malatjalian MD, Heidi Sapp MD and Laurette Geldenhuys MD (QEII Health Science Centre, Halifax NS, Canada) for independent expert histopathological review of esophageal tissue sections. We are also grateful to Tim May from the Canadian Light Source for design and construction of beamline 01B1-01 and to Tor Pedersen for constant help in maintaining it. The research described in this paper was performed at the Canadian Light Source, which is supported by NSERC, NRC, CIHR, and the University of Saskatchewan.

References

- 1 D. Forman, *Aliment Pharmacol Ther*, 2004, **20**, 6.
- 2 J. Lagergren, R. Bergstrom, A. Lindgren and O. Nyren, *New England Journal of Medicine*, 1999, **340**, 825–831.
- 3 S. T. Mayne, H. A. Risch, R. Dubrow, W. H. Chow, M. D. Gammon, T. L. Vaughan, D. C. Farrow, J. B. Schoenberg, J. L. Stanford, H. Ahsan, A. B. West, H. Rotterdam, W. J. Blot and J. F. Fraumeni, Jr., *Cancer Epidemiology, Biomarkers & Prevention*, 2001, **10**, 1055–1062.
- 4 P. J. Veugelers, G. A. Porter, D. L. Guernsey and A. G. Casson, *Diseases of the Esophagus*, 2006, **19**, 321–328.
- 5 D. C. Whiteman, S. Sadeghi, N. Pandeya, B. M. Smithers, D. C. Gotley, C. J. Bain, P. M. Webb and A. C. Green, for the Australian Cancer Study, *Gut*, 2008, **57**, 173–180.
- 6 A. Wong and R. C. Fitzgerald, *Clinical Gastroenterology & Hepatology*, 2005, **3**, 1–10.
- 7 N. Shaheen and D. F. Ransohoff, *JAMA*, 2002, **287**, 1972–1981.
- 8 S. J. Spechler, *New England Journal of Medicine*, 2002, **346**, 836–842.
- 9 D. T. McManus, A. Olaru and S. J. Meltzer, *Cancer Research*, 2004, **64**, 1561–1569.
- 10 B. J. Reid, P. L. Blount and P. S. Rabinovitch, *Gastrointestinal Endoscopy Clinics of North America*, 2003, **13**, 369–397.
- 11 C. P. Wild and L. J. Hardie, *Nature Reviews, Cancer*, 2003, **3**, 676–684.
- 12 E. Montgomery, M. P. Bronner, J. R. Goldblum, J. K. Greenson, M. M. Haber, J. Hart, L. W. Lamps, G. Y. Lauwers, A. J. Lazenby, D. N. Lewin, M. E. Robert, A. Y. Toledo, Y. Shyr and K. Washington, *Human Pathology*, 2001, **32**, 368–378.
- 13 R. D. Odze, *Journal of Clinical Pathology*, 2006, **59**, 1029–1038.
- 14 B. J. Reid, R. C. Haggitt, C. E. Rubin, G. Roth, C. M. Surawicz, G. Van Belle, K. Lewin, W. M. Weinstein, D. A. Antonioli and H. Goldman, *Human Pathology*, 1988, **19**, 166–178.
- 15 D. L. Chao, C. A. Sanchez, P. C. Galipeau, P. L. Blount, T. G. Paulson, D. S. Cowan, K. Ayub, R. D. Odze, P. S. Rabinovitch and B. J. Reid, *Clin Cancer Res*, 2008, **14**, 6988–6995.
- 16 A. M. Rygiel, F. Milano, F. J. Ten Kate, A. Schaap, K. K. Wang, M. P. Peppelenbosch, J. J. Bergman and K. K. Krishnadas, *Cancer Epidemiology, Biomarkers & Prevention*, 2008, **17**, 1380–1385.
- 17 E. Sabo, P. A. Meitner, R. Tavares, C. L. Corless, G. Y. Lauwers, S. F. Moss and M. B. Resnick, *Clin Cancer Res*, 2008, **14**, 6440–6448.
- 18 E. R. Blout and R. C. Mellors, *Science (Washington, D.C., U.S.)*, 1949, **110**, 137–138.
- 19 D. L. Woernley, *Cancer Res.*, 1952, **12**, 516–523.
- 20 F. Siebert and P. Hildebrandt, *Vibrational Spectroscopy in Life Science*, Wiley-VCH, Weinheim, 2007.
- 21 P. G. Andrus, *Technol. Cancer Res. Treat.*, 2006, **5**, 157–167.
- 22 S. Argov, J. Ramesh, A. Salman, I. Sinelnikov, J. Goldstein, H. Guterman and S. Mordechai, *J Biomed Opt*, 2002, **7**, 248–254.
- 23 V. Crupi, V. Venuti and D. Majolino, *Spectroscopy (Duluth, MN, U.S.)*, 2004, **19**(22), 24–30, 42.
- 24 *Vibrational Spectroscopy for Medical Diagnosis*, ed. M. Diem, P. R. Griffiths and J. M. Chalmers, John Wiley & Sons, Chichester, 2008.
- 25 M. Diem, M. Romeo, S. Boydston-White, M. Miljkovic and C. Matthaeus, *Analyst*, 2004, **129**, 880–885.
- 26 C. Krafft and V. Sergio, *Spectroscopy (Amsterdam, Neth.)*, 2006, **20**, 195–218.
- 27 Z. Movasagh, S. Rehman and I. u. Rehman, *Appl. Spectrosc. Rev.*, 2008, **43**, 134–179.
- 28 D. Naumann, *Appl. Spectrosc. Rev.*, 2001, **36**, 239–298.
- 29 R. K. Sabu and S. Mordechai, *Future Oncol.*, 2005, **1**, 635–647.
- 30 T. D. Wang, G. Triadafilopoulos, J. M. Crawford, L. R. Dixon, T. Bhandari, P. Sahbaie, S. Friedland, R. Soetikno and C. H. Contag, *Proc. Natl. Acad. Sci. USA*, 2007, **104**, 15864–15869.
- 31 M. Diem, S. Boydston-White and L. Chiriboga, *Appl. Spectrosc.*, 1999, **53**, 148A–161A.
- 32 D. E. Maziak, M. T. Do, F. M. Shamji, S. R. Sundaresan, D. G. Perkins and P. T. T. Wong, *Cancer Detect. Prev.*, 2007, **31**, 244–253.
- 33 B. Rigas, S. Morgello, I. S. Goldman and P. T. T. Wong, *Proc. Natl. Acad. Sci. USA*, 1990, **87**, 8140–8144.
- 34 P. T. T. Wong, M. K. Senterman, P. Jackli, R. K. Wong, S. Salib, C. E. Campbell, R. Feigel, W. Faught and M. F. K. Fung, *Biopolymers*, 2002, **67**, 376–386.
- 35 P. T. T. Wong, R. K. Wong, T. A. Caputo, T. A. Godwin and B. Rigas, *Proc. Natl. Acad. Sci. USA*, 1991, **88**, 10988–10992.
- 36 A. G. Casson, S. C. Evans, A. Gillis, G. A. Porter, P. Veugelers, S. J. Darnton, D. L. Guernsey and P. Hainaut, *Journal of Thoracic & Cardiovascular Surgery*, 2003, **125**, 1121–1131.
- 37 A. G. Casson, Z. Zheng, S. C. Evans, L. Geldenhuys, S. V. van Zanten, P. J. Veugelers, G. A. Porter and D. L. Guernsey, *Cancer*, 2005, **104**, 730–739.
- 38 A. G. Casson, Z. Zheng, S. C. Evans, P. J. Veugelers, G. A. Porter and D. L. Guernsey, *Carcinogenesis*, 2005, **26**, 1536–1541.
- 39 L. Chiriboga, P. Xie, H. Yee, D. Zarou, D. Zakim and M. Diem, *Cell. Mol. Biol. (Paris)*, 1998, **44**, 219–229.
- 40 L. Chiriboga, P. Xie, H. Yee, V. Vigorita, D. Zarou, D. Zakim and M. Diem, *Biospectroscopy*, 1998, **4**, 47–53.
- 41 T. D. Wang, G. Triadafilopoulos, J. M. Crawford, L. R. Dixon, T. Bhandari, P. Sahbaie, S. Friedland, R. Soetikno and C. H. Contag, *Proc. Natl. Acad. Sci. USA*, 2007, **104**, 15864–15869.
- 42 L. A. Liotta and E. C. Kohn, *Nature (London, U.K.)*, 2001, **411**, 375–379.
- 43 L. C. L. T. van Kempen, D. J. Ruiter, G. N. P. van Muijen and L. M. Coussens, *European journal of cell biology*, 2003, **82**, 539–548.
- 44 L. Chiriboga, P. Xie, V. Vigorita, D. Zarou, D. Zakim and M. Diem, *Biospectroscopy*, 1998, **4**, 55–59.
- 45 L. Chiriboga, P. Xie, W. Zhang and M. Diem, *Biospectroscopy*, 1997, **3**, 253–257.
- 46 L. Chiriboga, H. Yee, M. Diem and B. Wood, *Gynecol Oncol*, 2003, **91**, 275–276; author reply: F. K. Lim, S. Neviliappan and P. T. T. Wong, *Gynecol Oncol*, 2003, **91**, 276–277.